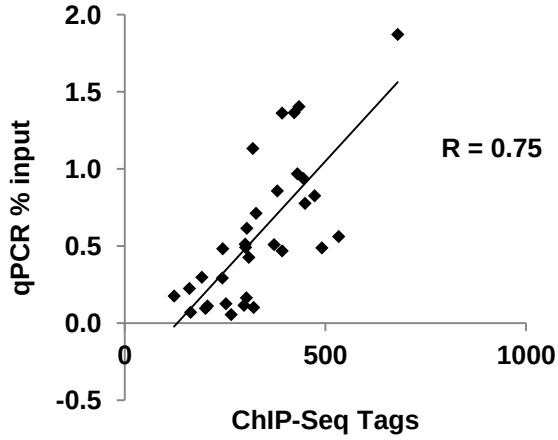


**Figure S1. Correlation between ChIP-seq tag intensity and ChIP-qPCR.** 30 randomly ARBS were selected from the DHT ChIP-seq library for ChIP-qPCR analysis.

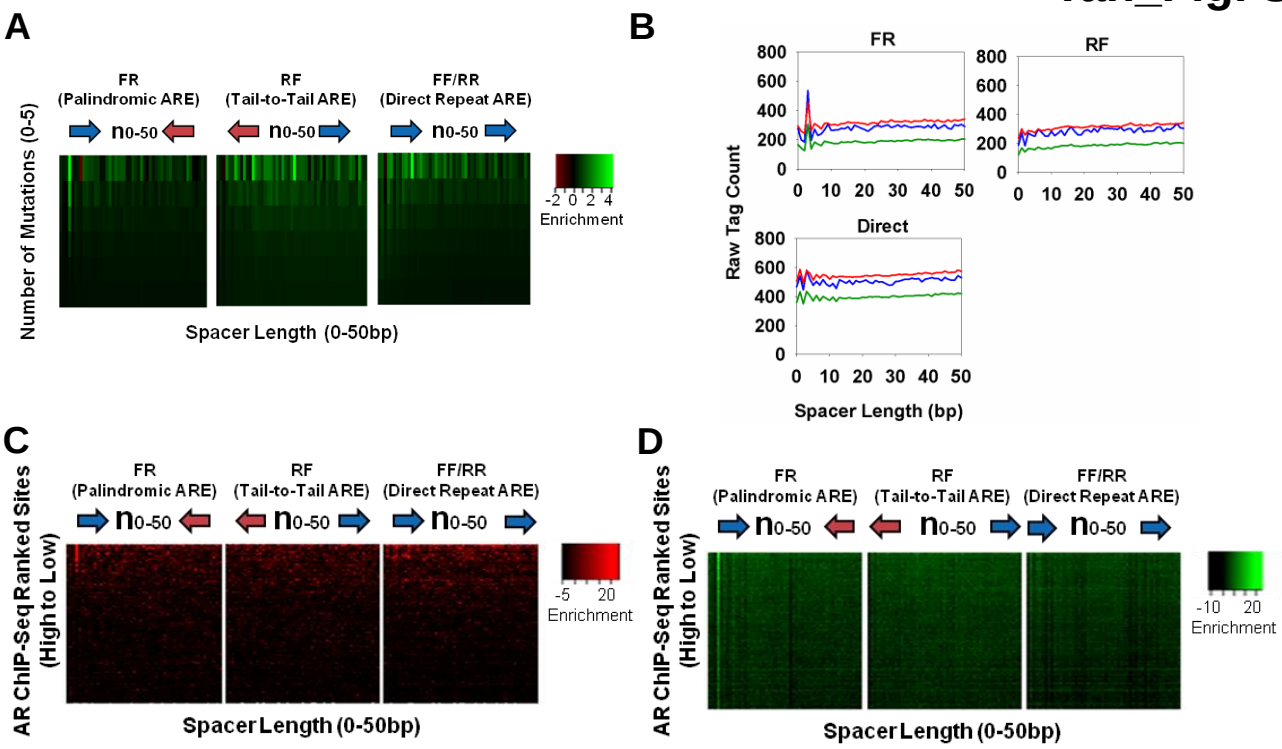


**Figure S2. Characterization of ARE configurations in ARBS.**

(A) Heatmap of ARE configurations. Putative ARBS of 400 bp from ChIP-seq data was scanned for different possible configurations (ie. 0-5 mutations from canonical ARE with varying spacer length ranging from 0-50 bp). The heatmap was generated using logarithm of the raw count of each configuration within all ARBS over the background. Background comparison was generated by random scrambling of half ARE positions for each binding site. (B) Bootstrap analysis to determine ARE configurations associated with stronger AR binding. The observed statistics represent number of sites within the top 1,000 AR ChIP-seq ranked sites of 400 bp having different ARE configurations. 1,000 sites were randomly picked a million times (blue graph) from the top 25,000 ranked sites in an iterative manner to achieve a confidence interval (CI) of 99.9999% (upper CI = red graph; lower CI = green graph). (C-D) To further evaluate if binding affinity is associated with ARE configurations, we sorted ARBS according to their tag intensity and then scanned these sites for possible ARE configuration with varying spacer length (0-50 bp). To generate the background, we repeated this procedure on 1 million set of 1,000 regions picked randomly from the (C) AR ChIP-seq library or (D) genomic DNA . We calculated the p-value of these 1,000 ARBS moving average. Heatmap was generated using logarithm of the calculated p-value (p-value raw count vs self).

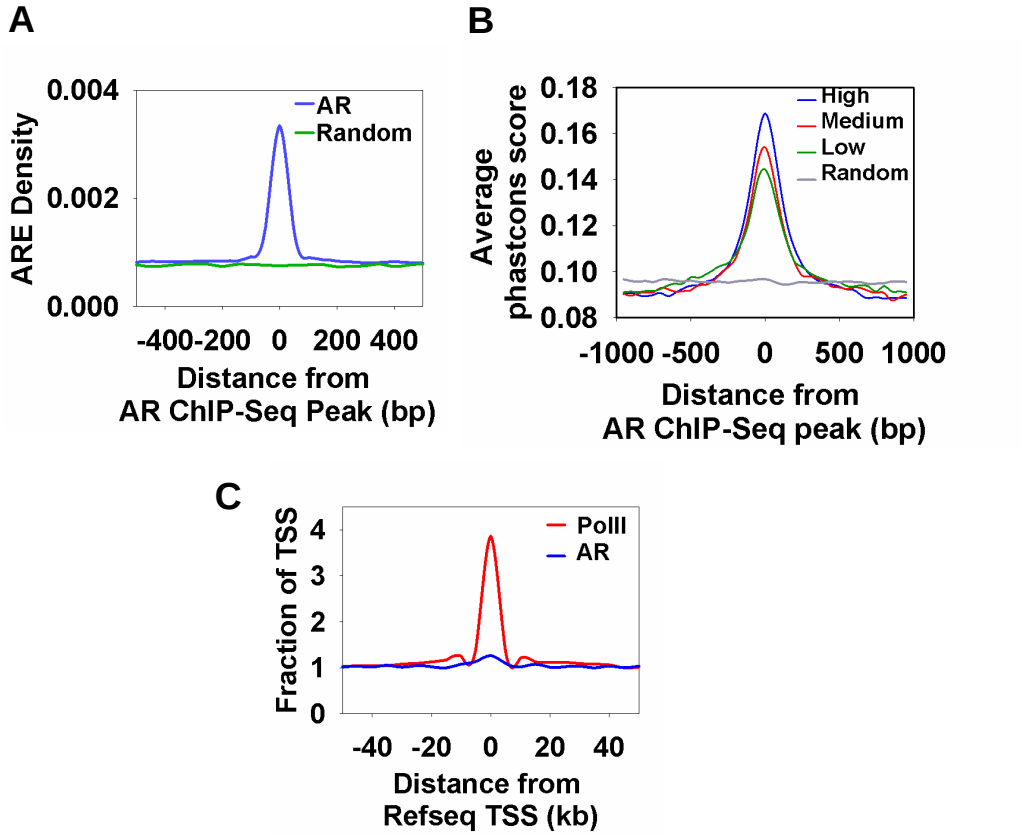


**Figure S3. Genomic analyses of ARBS in DHT-treated AR ChIP-seq libraries.**

(A) Distribution of canonical AREs in ARBS. (B) Evolutionary importance of ARBS. ARBS were first sorted according to tag intensity and equally then divided into three groups (high tags=blue line; medium tags=red line; low tags=green line). The mean PhastCons sequence conservation score (alignment of 16 vertebrate genomes with human) for every position in a 2,000 bp window around the ChIP-seq peaks from the DHT-treated AR library was then plotted for each group in comparison with randomly selected genomic regions (grey line). (C) Distribution of ARBS and RNA Pol II binding sites found within 50 kb of the TSS of RefSeq genes.

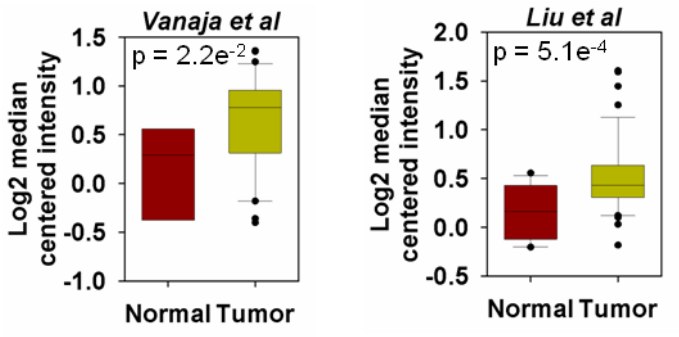


**Figure S4. NKX3-1 expression in normal and prostate tumor samples.** Box-plots illustrating Oncomine database analysis of NKX3-1 gene expression in normal and prostate carcinoma samples (studies by Liu *et al*. and Vanaja *et al*.). The differential gene expression data is centered on the median of expression levels on a log2 scale. The p-value was calculated using the Welch two sample t-test.

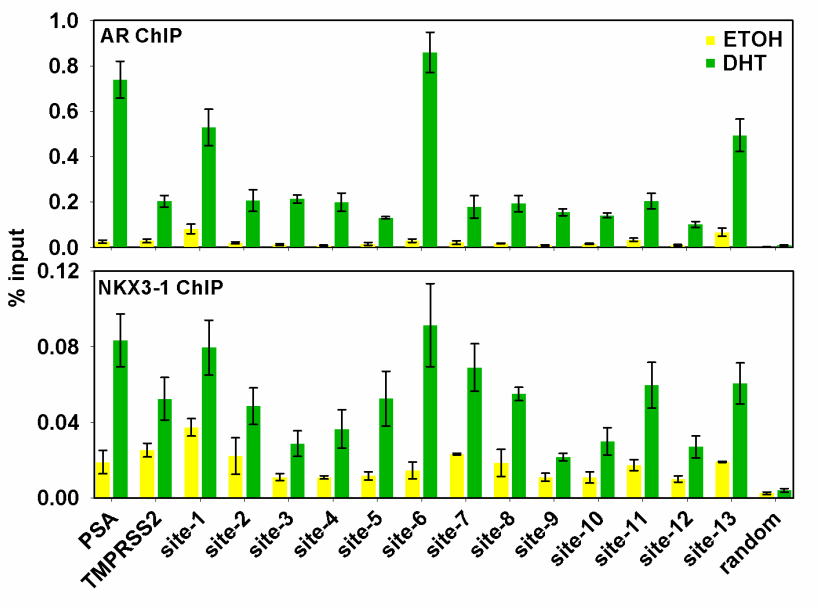


**Figure S5. NKX3-1 is co-localization at ARBS.** Androgen-depleted LNCaP cells were treated with ETOH or 100 nM DHT for 2 hrs followed by ChIP assay performed with antibody against AR (top panel) or NKX3-1 (bottom panel). Immunoprecipitated DNA was amplified by real-time qPCR using primers spanning sites with AR and NKX3-1 co-occupancies as well as a randomly selected genomic control site which is not bound by both proteins. The results are represented as the mean ± SEM of triplicate experiments.

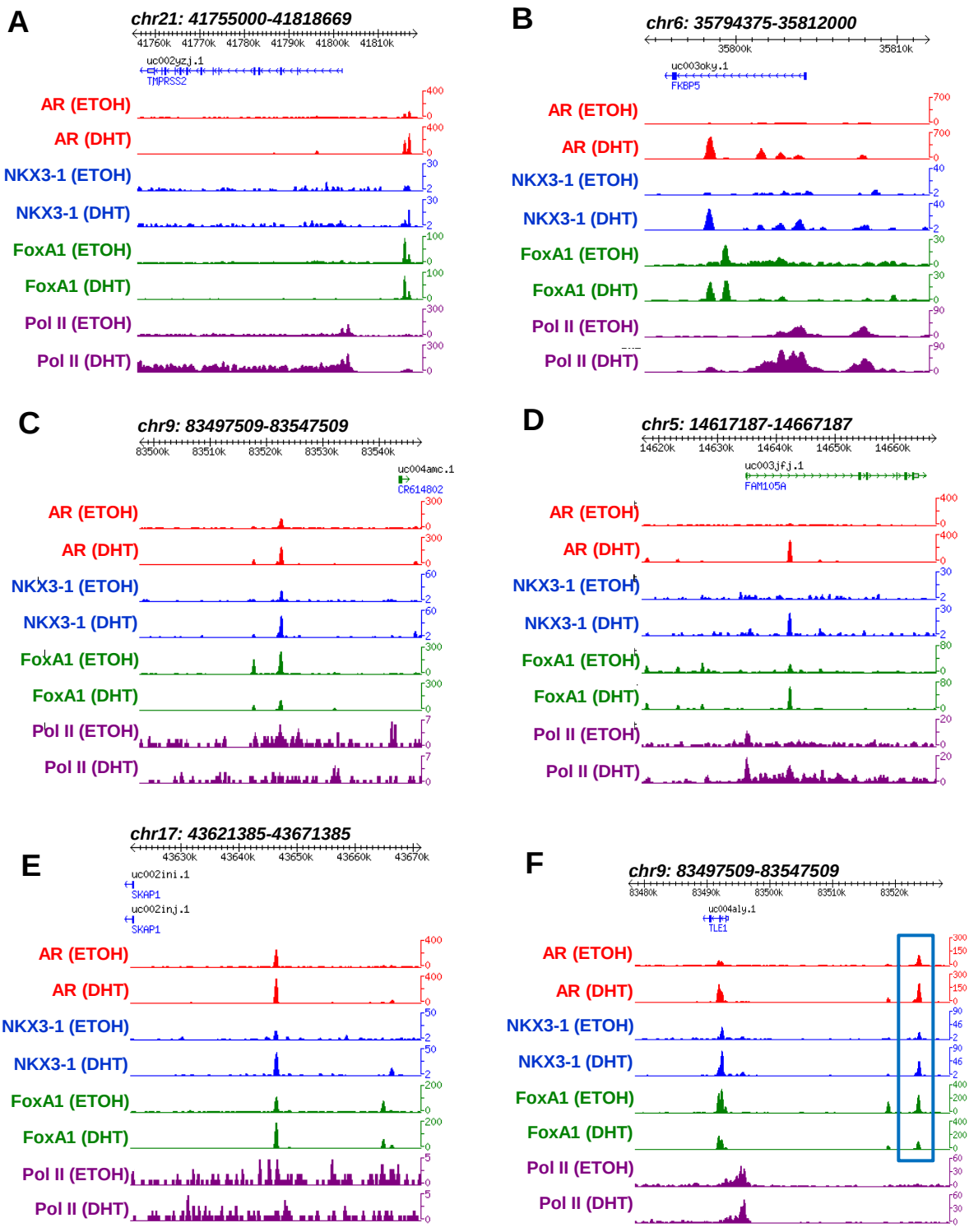


**Figure S6. Co-localization of AR, NKX3-1, FoxA1, and RNA Pol II at well characterized model genes and other genomic regions.** Screenshots showing ChIP-seq rof the four factors before and after DHT stimulation near androgen-regulated genes such as (A) TMPRSS2 and (B) FKBP5 as well as (C-E) random genomic regions and (F) ARBS8.

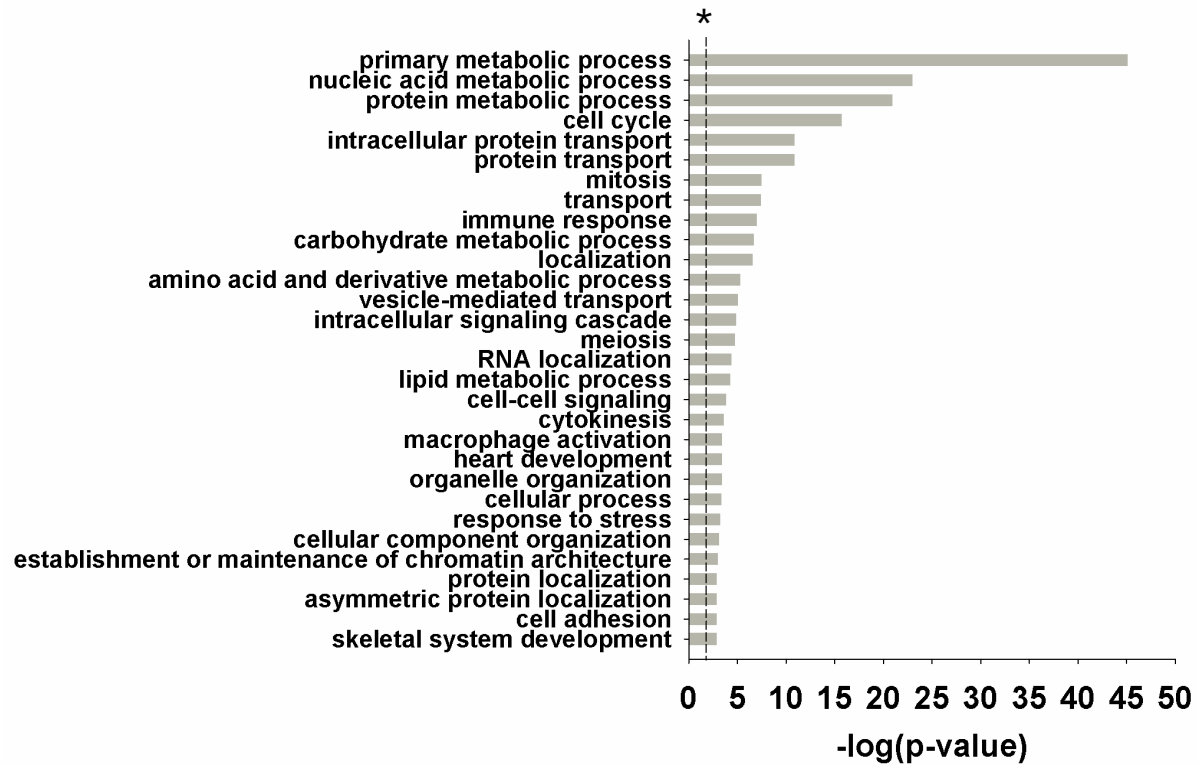


**Figure S7. Panther GO analysis of genes associated with ARBS (lacking NKX3-1).** GO analysis of androgen-dependent genes occupied by AR but exclusive of NKX3-1 within 50 kb of the TSS using the Panther webtool. *Threshold was set at a p-value of 0.01.

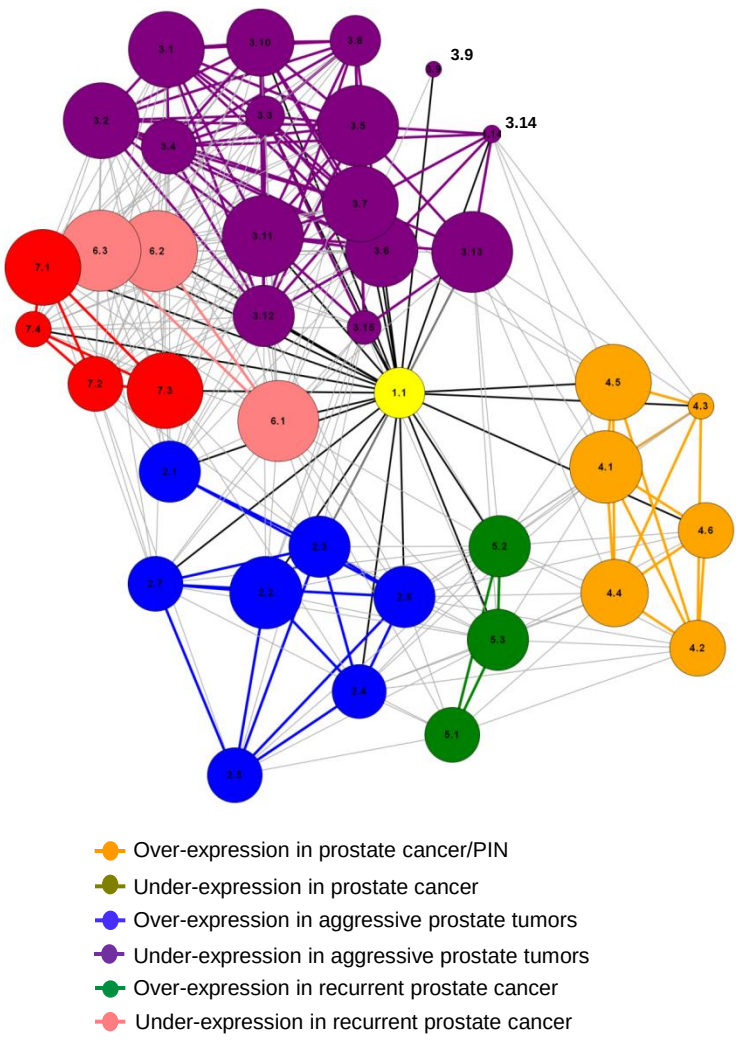


| Label | Concept Name |
|---|---|
| 1.1 | AR associated genes |
| 2.1 | Advanced Gleason Score (Best Prostate 2) |
| 2.2 | Advanced Gleason Score (Vanaja Prostate) |
| 2.3 | Metastasis (Best Prostate 2) |
| 2.4 | Metastasis (Varambally Prostate) |
| 2.5 | Advanced Gleason Score (Lapointe Prostate) |
| 2.6 | Advanced Gleason Score (Liu Prostate) |
| 2.7 | Advanced Stage (Lapointe Prostate) |
| 3.1 | Advanced Gleason Score (Luo Prostate 2) |
| 3.11 | Advanced Gleason Score (Taylor Prostate 3) |
| 3.1 | Advanced Stage (Bittner Prostate) |
| 3.12 | Advanced Stage (Glinsky Prostate) |
| 3.13 | Advanced Stage (Taylor Prostate 3) |
| 3.14 | Advanced Gleason Score (Tomlins Prostate) |
| 3.15 | Metastasis (Holzbeierlein Prostate) |
| 3.2 | Advanced Grade (Bittner Prostate) |
| 3.3 | Metastasis (Holzbeierlein Prostate) |
| 3.4 | Metastasis (Lapointe Prostate) |
| 3.5 | Metastasis (Taylor Prostate 3) |
| 3.6 | Metastasis (Vanaja Prostate) |
| 3.7 | Metastasis (Varambally Prostate) |
| 3.8 | Metastasis (Yu Prostate) |
| 3.9 | Advanced Gleason Score (Welsh Prostate) |
| 4.1 | PCA (Vanaja Prostate) |
| 4.2 | PCA (Tomlins Prostate) |
| 4.3 | PCA (Taylor Prostate 3) |
| 4.4 | PCA (Luo Prostate 2) |
| 4.5 | PCA (Varambally Prostate) |
| 4.6 | PIN (Tomlins Prostate) |
| 5.1 | Recurrence at 1 Year (Lapointe Prostate) |
| 5.2 | Recurrence at 3 Years (Glinsky Prostate) |
| 5.3 | Recurrence at 5 Years (Glinsky Prostate) |
| 6.1 | Recurrence at 1 Year (Taylor Prostate 3) |
| 6.2 | Recurrence at 3 Years (Taylor Prostate 3) |
| 6.3 | Recurrence at 5 Years (Taylor Prostate 3) |
| 7.1 | PCA (Arredouani Prostate) |
| 7.2 | PCA (Lapointe Prostate) |
| 7.3 | PCA (Varambally Prostate) |
| 7.4 | PCA (LaTulippe Prostate) |

**Figure S8. Clinical parameters enriched for genes associated with AR.** Oncomine Concepts Map analysis illustrating the enrichment network between AR-associated genes and gene signatures in different prostate carcinoma subtypes. Top differentially regulated genes were considered to allow similar gene set size as AR and NKX3-1 co-bound genes. Each node represents one molecular concept with the node size proportional to the number of genes within each gene set. Statistically significant overlap ($p < 0.01$) between genes in two linked nodes is represented by an edge. Concepts were categorized into 7 major clusters as indicated by the different colors. Clinical studies found to be significantly associated with AR are listed on the right.

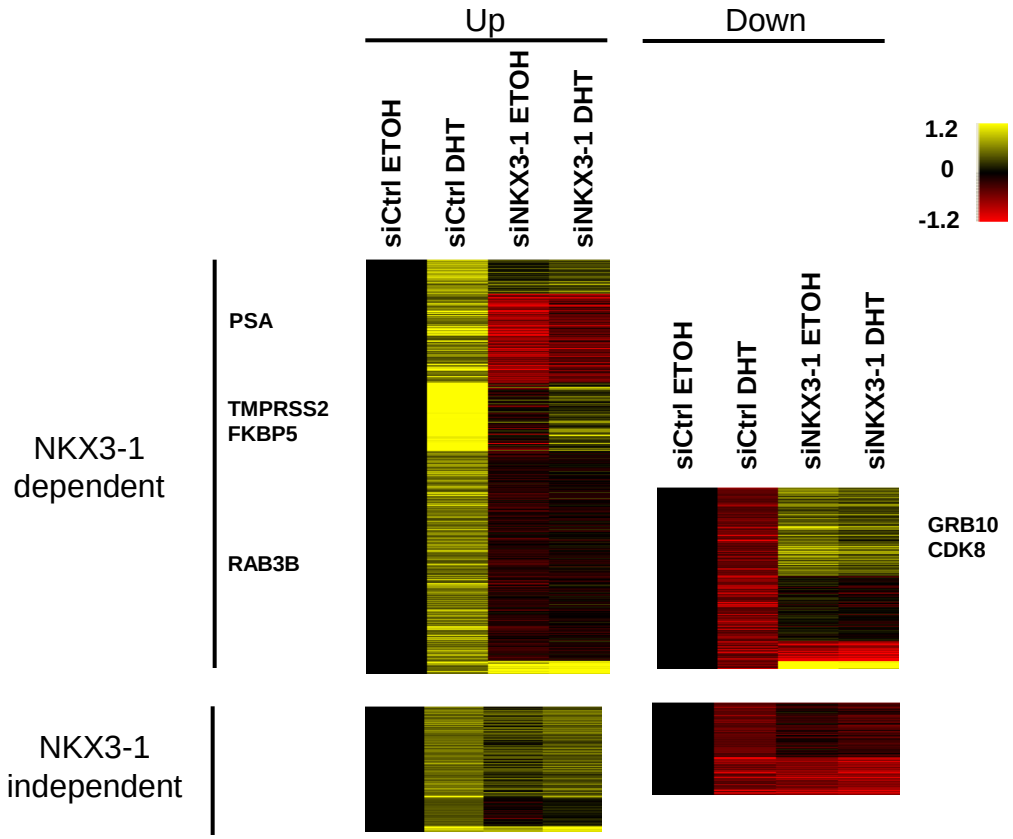


**Figure S9. Gene expression profile of androgen-regulated genes after NKX3-1 silencing.**

LNCaP cells were transfected with control or NKX3-1 siRNA before 10 nM DHT stimulation for 8 hr. The heatmap shows the gene expression profile of all DHT-regulated genes in which induction and repression relatively to ETOH treated siCtrl condition are represented by yellow and red shades, respectively. Genes were considered NKX3-1-dependent if their transcript level changed by at least 1.3-fold between DHT-treated siCtrl and siNKX3-1 conditions. Overall, 77% of DHT up-regulated genes and 66% down-regulated genes were affected by the loss of NKX3-1. Representative genes of AR which were affected by NKX3-1 silencing are listed at the side. All results represent the average of 3 independent experiments ±S.E.M.

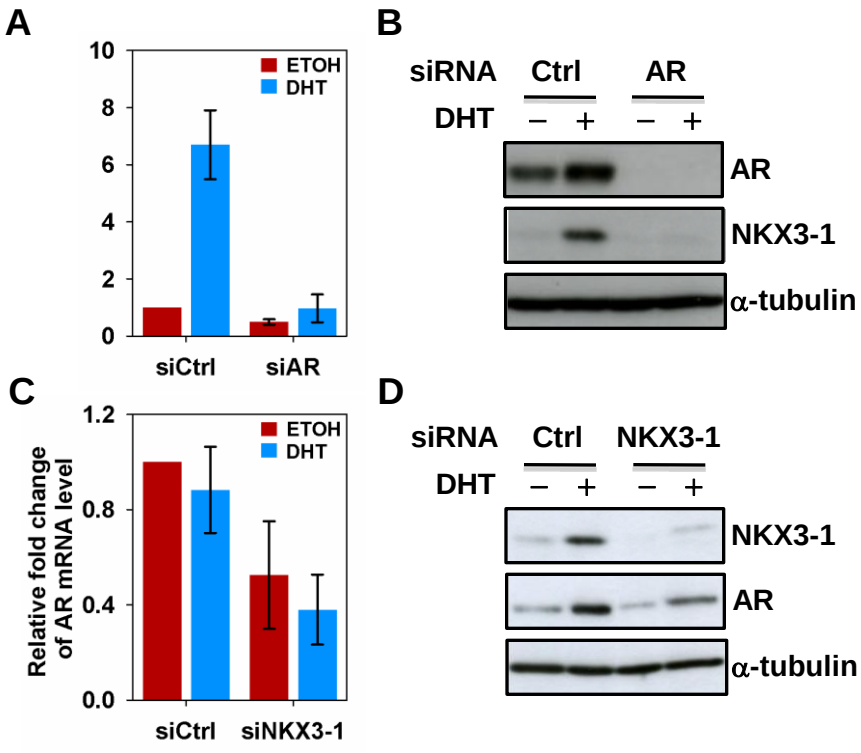


**Figure S10. Positive transcriptional regulation between AR and NKX3-1.**

To eliminate the likelihood of off-target knockdown effects for AR and NKX3-1, these genes were silenced independently with different siRNAs (siAR #2 and siNKX3-1 #2), before treating the cells with ETOH or 10 nM of DHT for 8 hrs. Total RNA was then isolated and then amplified with real-time RT-qPCR primers designed against the (A) AR and (B) NKX3-1 genes. All mRNA expression levels were normalized against GAPDH. The results are shown as the mean ±SEM of at least 3 independent experiments. (B and D) Protein levels of AR, NKX3-1 and loading control α-tubulin were assessed by Western blotting.

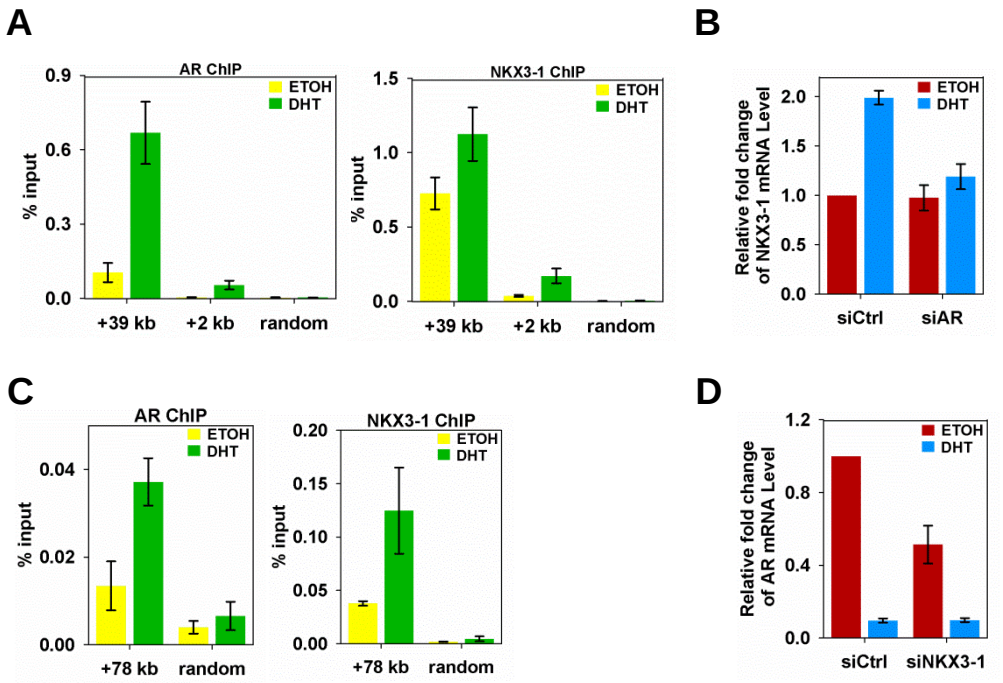


**Figure S11. AR and NKX3-1 directly regulate each others expression in VCaP cells.** (A) Androgen depleted VCaP cells were treated with ETOH or 100 nM DHT for 2 hr prior to harvesting for ChIP assay. ChIP-qPCR of AR and NKX3-1 was assessed at the enhancer and promoter of NKX3-1 gene. (B) Effect of AR silencing on NKX3-1 expression level. Hormone-depleted cells were transfected with either control siRNA or siRNA targeting AR before treatment with ETOH or 10 nM of DHT for 8 hr. Total RNA was isolated and amplified with real-time RT-qPCR primers of NKX3-1. mRNA expression levels were normalized against GAPDH. (C) ChIP-qPCR of AR and NKX3-1 at the AR gene. (D) Effect of NKX3-1 depletion on AR transcript level. Total RNA was isolated and amplified with real-time RT-qPCR primers of AR. mRNA expression levels were normalized against GAPDH. Data represents the mean ± SEM of at least three independent experiments.

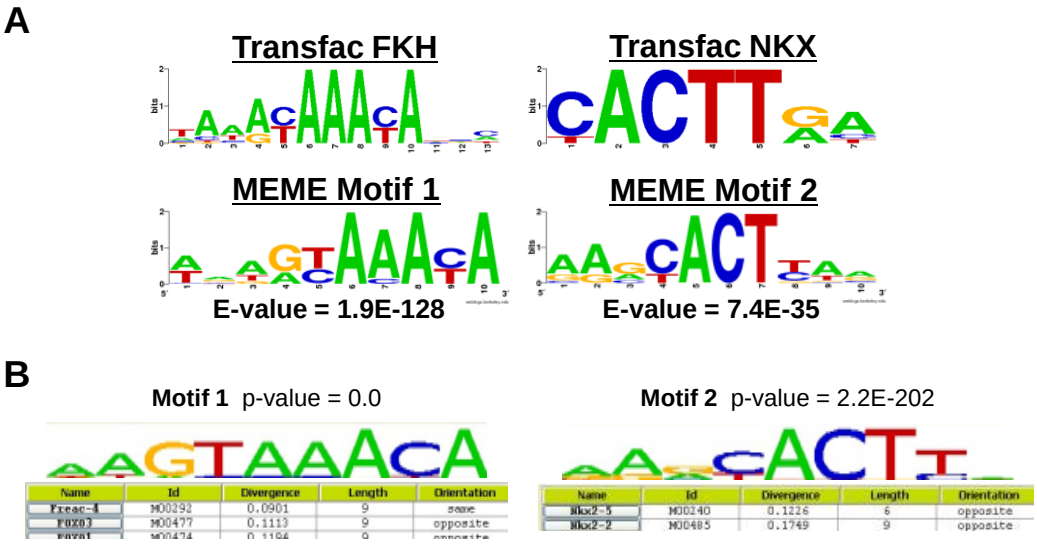


**Figure S12. Motif enrichment analysis of NKX3-1 binding sites.** (A) Top panel shows the Transfac weblogos for the HFH3 (left) and NKX2-5 (right) motifs. Bottom panel shows the MEME output for the top 500 NKX3-1 (DHT) ChIP-seq ranked binding sites (+/- 50 bp from ChIP-seq peak). (B) Top 2 motifs obtained when all the NKX3-1 (DHT) ChIP-seq binding sites (+/- 100 bp from ChIP-Seq peak) were analyzed by Amadeus, another de novo motif discovery program.

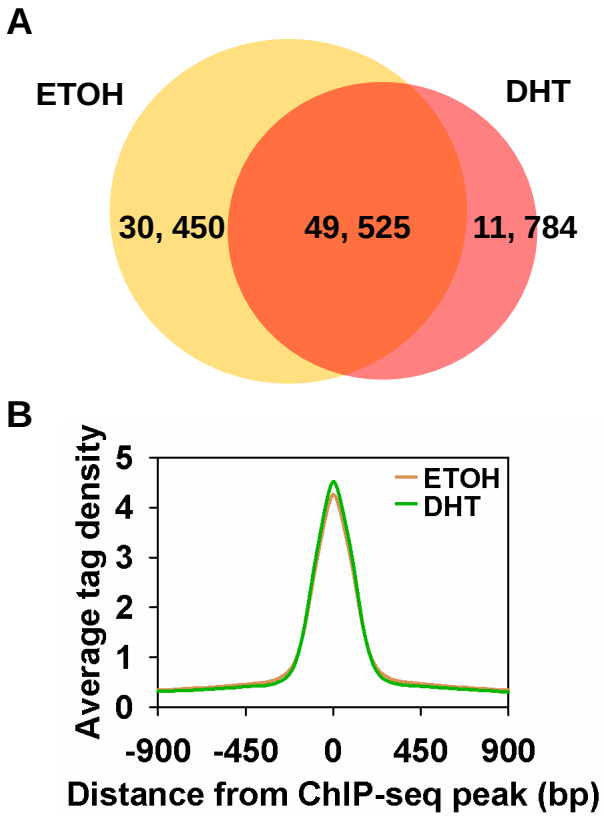


**Figure S13. Genomic binding of FoxA1 in LNCaP cells.** (A) Venn diagram showing the overlap between ETOH and DHT treated FoxA1 ChIP-seq peaks. (B) FoxA1 ChIP-seq tag distribution around AR (DHT) binding sites.

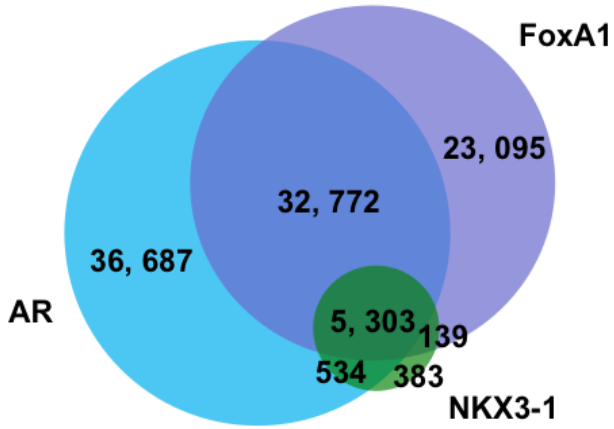


**Figure S14. Venn diagram showing the overlap between androgen-stimulated AR, FoxA1, and NKX3-1 binding sites.**

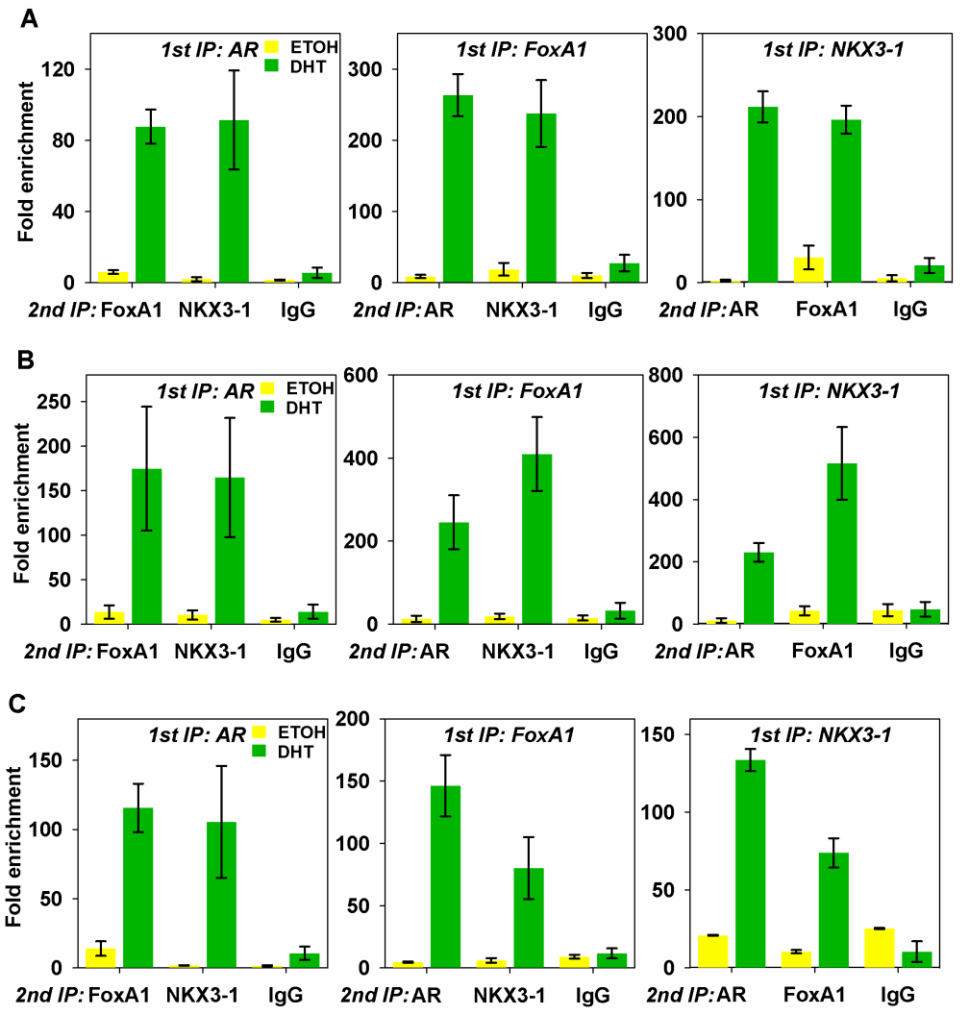


**Figure S15. Sequential ChIP of AR, NXK3-1, and FoXA1.** (A-C) Sequential ChIP analysis of AR, NKX3-1, and FoxA1 was performed on three genomic regions (as shown in Figs. S6C-E) where the three factors are co-localized. The experimental results are presented as the mean ±SEM of at least 3 independent assays.

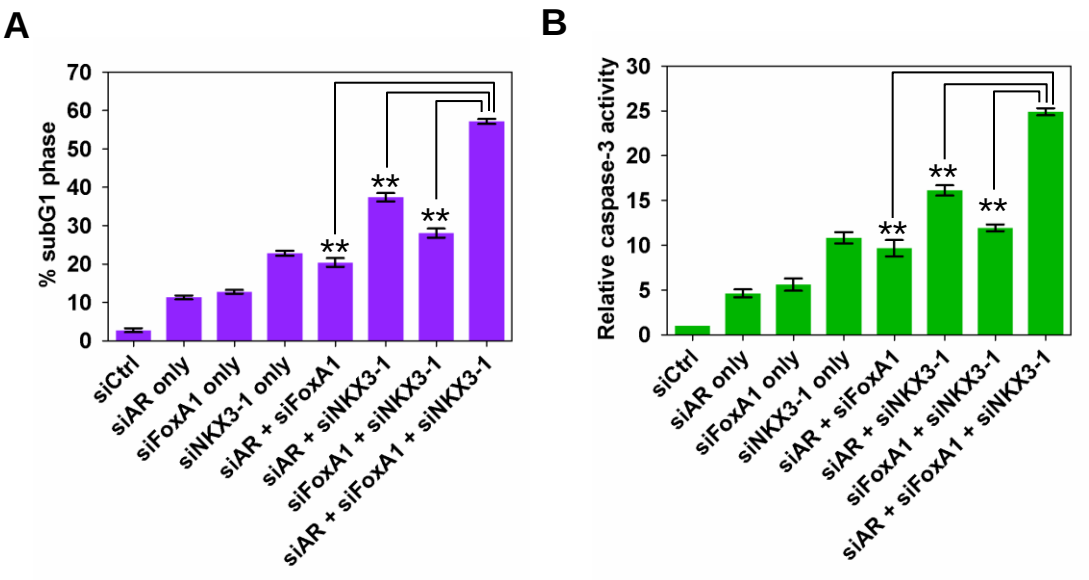


**Figure S16. Cell death assays to demonstrate the effects of knockdown in LNCaP cells under serum condition**. AR, FoxA1 and NKX3-1 were silenced by siRNA in various combinations in LNCaP cells under serum condition. (A) Cells were stained with PI and analyzed using flow cytometry as described in Fig. 5E. (B) Cells were assayed for caspase-3 activity as described in Fig. 5F.

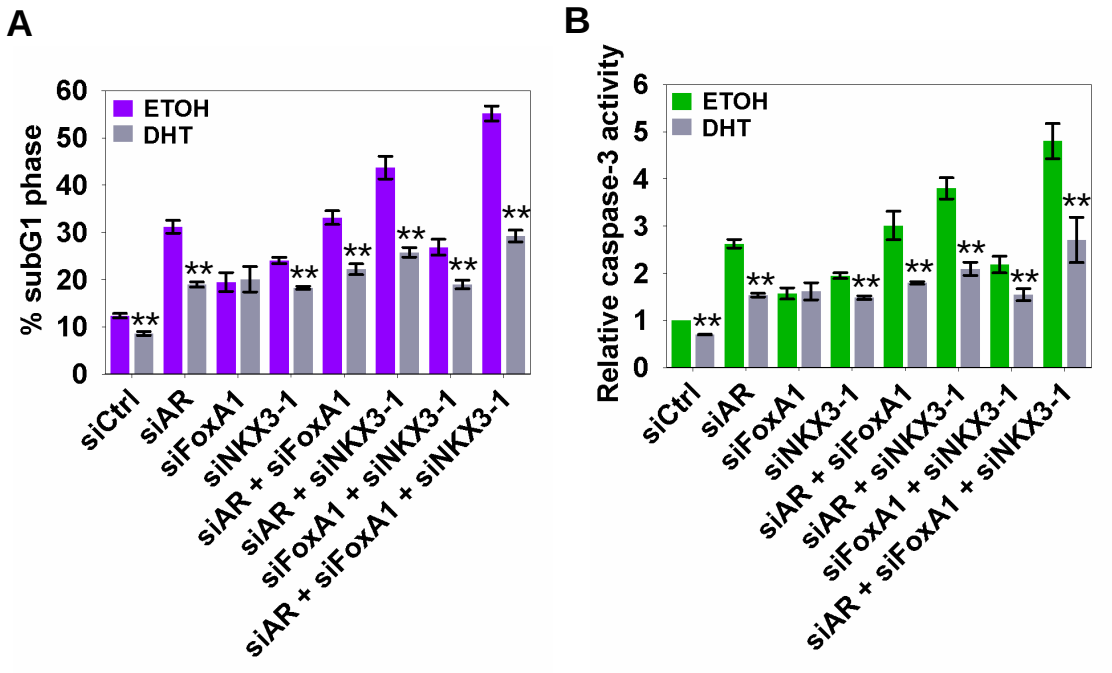


**Figure S17. Cell death assays to assess the effects of AR, FoxA1 and NKX3-1 depletion in VCaP cells upon DHT stimulation.** VCaP cells were depleted of AR, FoxA1, or NKX3-1 singly or in combination followed by ETOH or DHT treatment for 48 hr. (A) Cells were stained with propidium iodide and analyzed using flow cytometry as described in Fig. 5E. (B) Cells were assayed for caspase-3 activity as described in Fig. 5F.

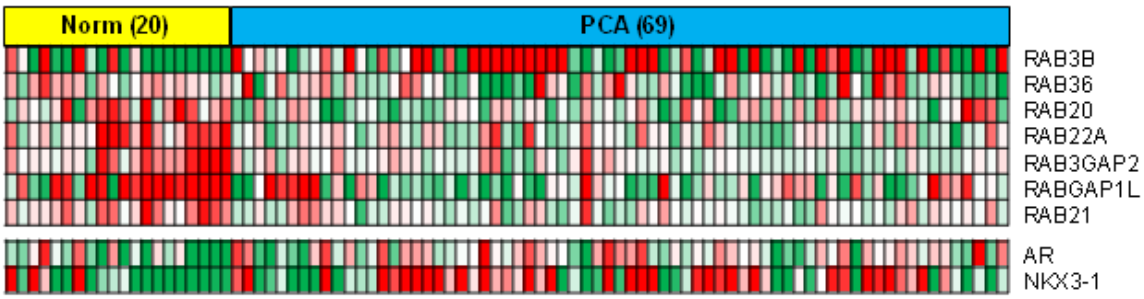


**Figure S18. Expression of RAB GTPase genes in normal and prostate tumors.** Heatmap showing an overview of the expression patterns of RAB GTPase genes as well as AR and NKX3-1 from the study by Wallace *et al*. The samples are categorized into normal vs prostate adenocarcinoma. Red and green boxes represent over- and under-expression normalized to the tumor microarray reference probe, respectively.

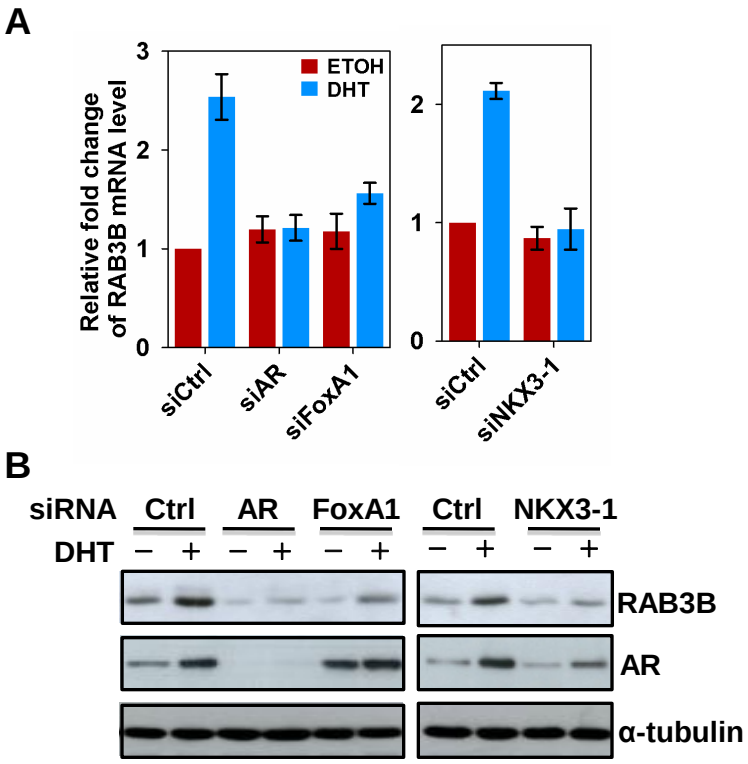


**Figure S19. Effect of AR, NKX3-1, and FoxA1 silencing on RAB3B and AR expression in LNCaP cells.** AR, NKX3-1 and FoxA1 were silenced independently in androgen-deprived LNCaP cells before treatment with either ETOH or 10 nM of DHT for 8 hrs. (A) Total RNA was then isolated and amplified with real-time RT-qPCR primers designed against the Rab3B gene. All mRNA expression levels were normalized against that of GAPDH. The data are presented as the mean ±SEM of at least 3 independent experiments. (B) Effect of transcription factor depletion on Rab3B and AR protein levels was assessed by western blotting.

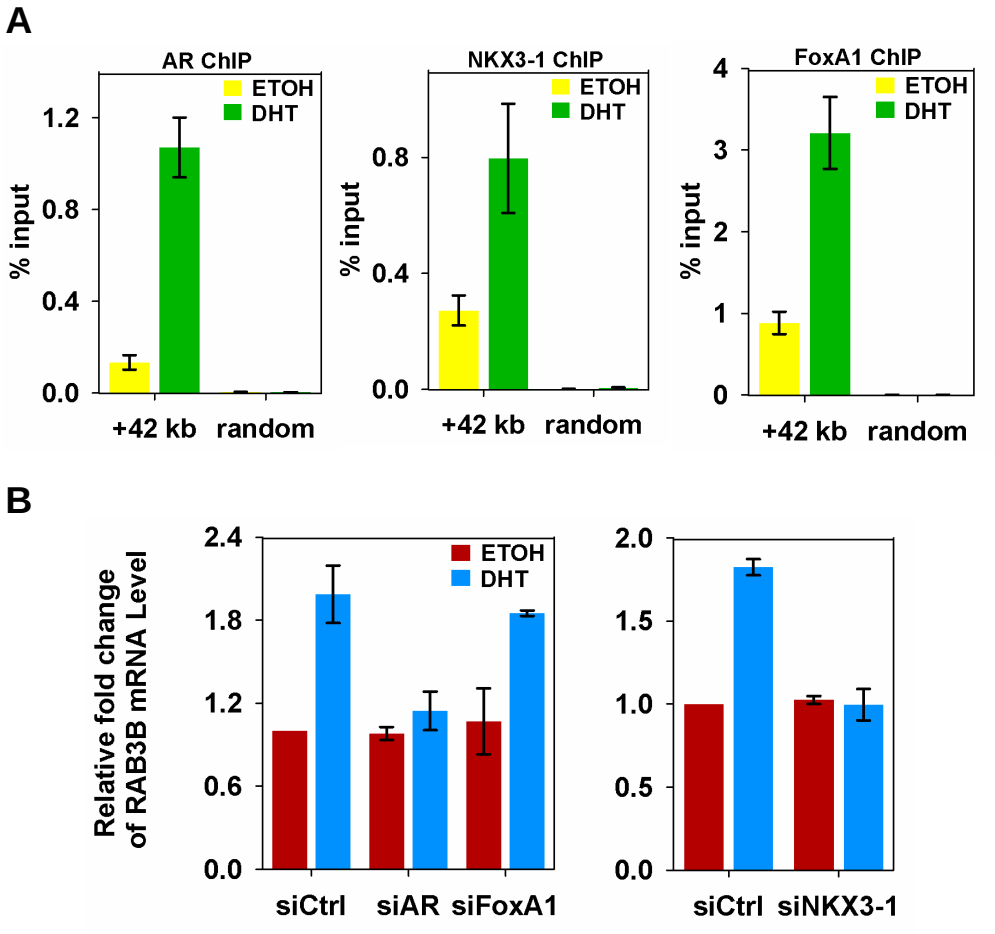


**Figure S20. AR and NKX3-1 regulate RAB3B gene expression in VCaP cells.** (A) ChIP-qPCR of AR, NKX3-1, and FoxA1 at the enhancer region of the Rab3B gene. (B) AR, NKX3-1, and FoxA1 were depleted in androgen deprived VCaP cells before 8 hr treatment with either ETOH or 10 nM DHT. Total RNA was then isolated and amplified with real-time RT-qPCR primers designed against the Rab3B gene. All mRNA expression levels were normalized against that of GAPDH. The data are presented as the mean ±SEM of at least 3 independent experiments.

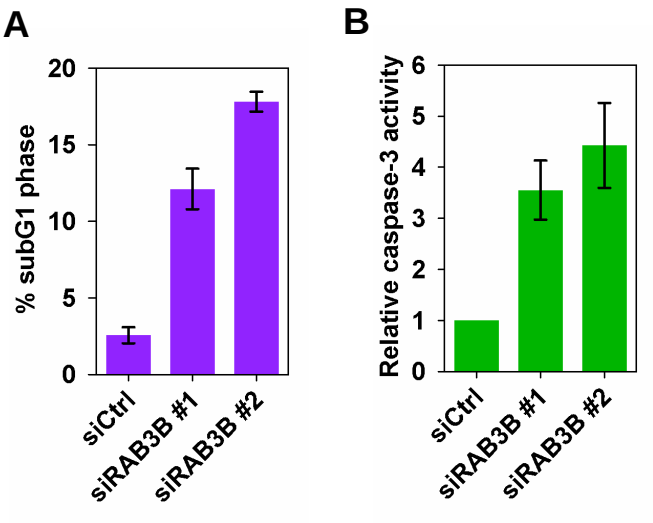


**Figure S21. Cell death assays to assess RAB3B silencing in LNCaP cells under serum condition.** LNCaP cells were depleted of RAB3B in serum condition. (A) Cells were stained with propidium iodide and analyzed using flow cytometry as described in Fig. 5E. (B) Cells were assayed for caspase-3 activity as described in Fig. 5F. Data are presented as the mean ± SEM of triplicate experiments.

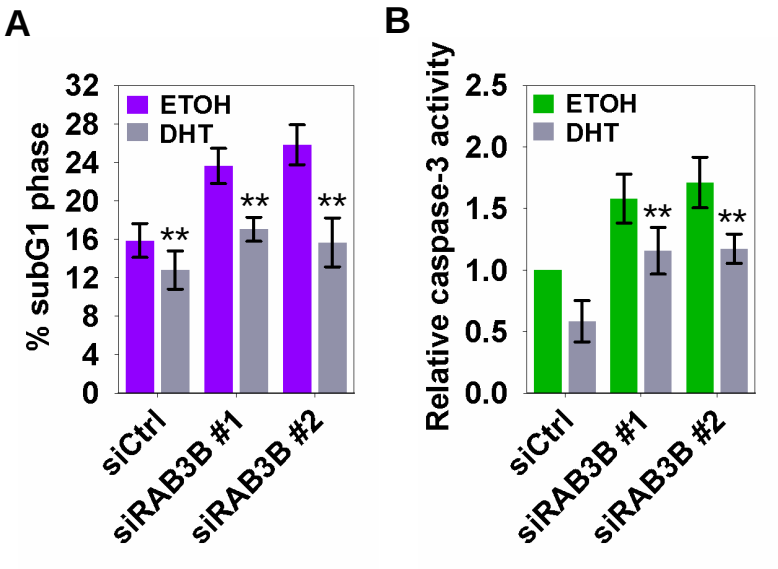


**Figure S22. Cell death assays to assess RAB3B silencing in VCaP cells under serum condition.** Rab3B gene expression was suppressed in VCaP cells under serum condition. (A) Cells were stained with propidium iodide and analyzed using flow cytometry as described in Fig. 5E. (B) Cells were assayed for caspase-3 activity as described in Fig. 5F. Data are presented as the mean ± SEM of triplicate experiments. Statistical analysis was performed for difference between ETOH and DHT conditions using the Student's t test where ** $p < 0.05$.

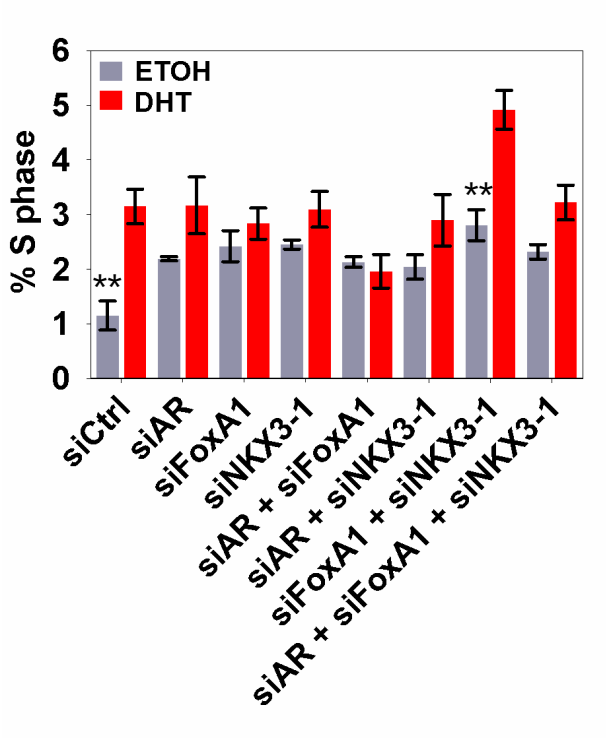


**Figure S23. Effect of AR, NKX3-1, and FoxA1 silencing on LNCaP cell proliferation.** AR, NKX3-1, and FoxA1 were silenced either individually or in various combinations in androgen deprived LNCaP cells before treatment with either ETOH or 100 nM of DHT for 72 hr. Cells were stained with propidium iodide and analyzed using flow cytometry. Analysis was represented as % S-phase based on % of total number of gated cells within the S-phase. Data are presented as the mean ±SEM of triplicate experiments. Statistical analysis was performed for differences between ETOH and DHT conditions using the Student's t-test where ** $p < 0.05$.

| | | Unique Tags | Peaks |
|---|---|---|---|
| **AR** | **ETOH** | 17,413,241 | 18,117 |
| | **DHT** | 13,252,823 | 75,296 |
| **NKX3-1** | **ETOH** | 9,622,573 | - |
| | **DHT** | 9,500,116 | 6,359 |
| **FoxA1** | **ETOH** | 13,462,620 | 79,975 |
| | **DHT** | 8,677,867 | 61,309 |
| **PolII** | **ETOH** | 10,003,579 | 113,274 |
| | **DHT** | 9,045,771 | 104,025 |

**Table S1. AR, NKX-31, FoxA1, and RNA pol II ChIP-seq library information.** Summary of unique tag counts and total number of peaks called using FDR 0.05 for each ChIP-seq library.

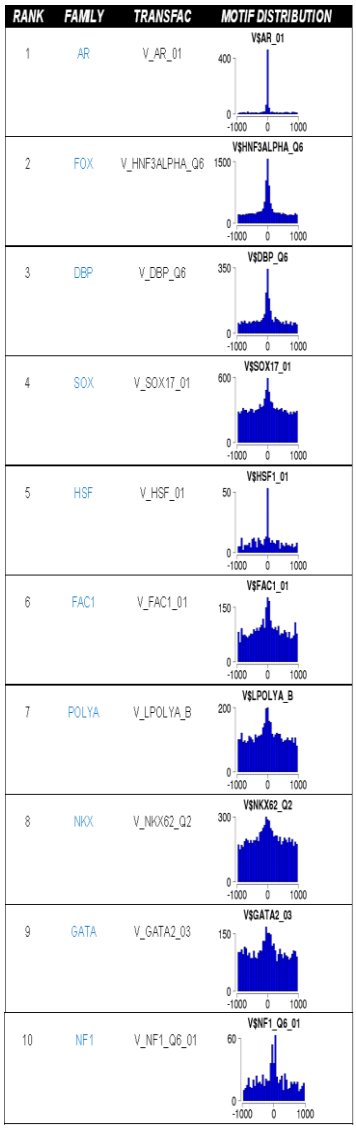


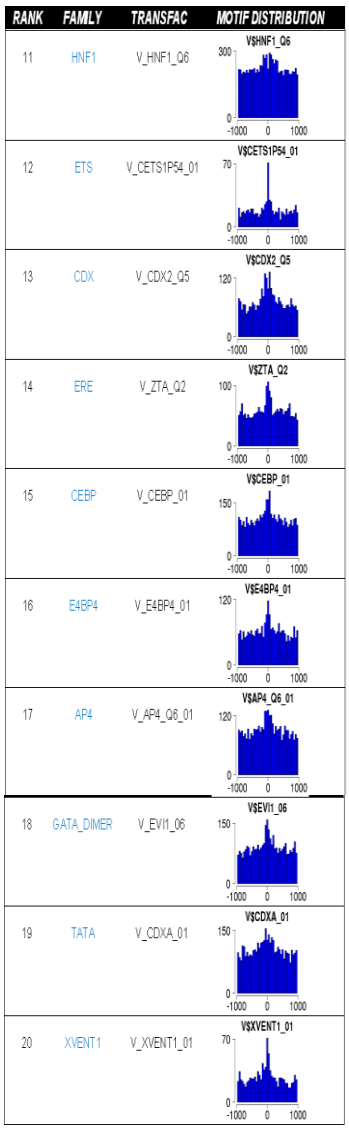


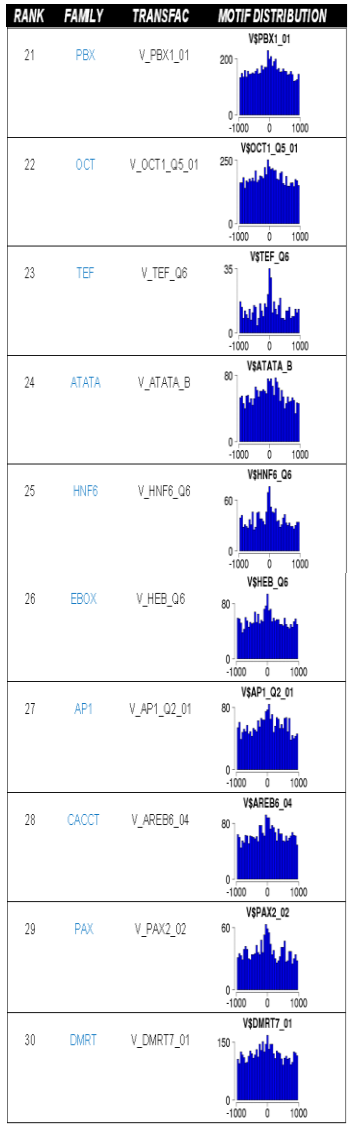


**Table S2. CENTDIST analysis of ARBS.** CENTDIST was performed on the top 10,000 ARBS (DHT). Shown here is the motif distribution result for the top 30 ranked transcription factor family members.